Negative Dielectric Constant and Electrical Conductivity of Au/*n*-Si (111) Schottky Barrier Diodes with PVA/Ni,Zn Interfacial Layer

T. Tunç,[1] İ. Dökme,[2] Ş. Altındal,[3] İ. Uslu[4]

[1]*Science Education Department, Faculty of Education, Aksaray University, Aksaray, Turkey*
[2]*Science Education Department, Faculty of Gazi Education, Gazi University, Ankara, Turkey*
[3]*Physics Department, Faculty of Arts and Sciences, Gazi University, Ankara, Turkey*
[4]*Chemistry Education Department, Faculty of Education, Gazi University, Ankara, Turkey*

Received 28 April 2010; accepted 21 December 2010
DOI 10.1002/app.34029
Published online 21 April 2011 in Wiley Online Library (wileyonlinelibrary.com).

ABSTRACT: In this study, the dielectric properties and alternating-current (ac) conductivity of Au/(PVA/Ni,Zn acetates)/*n*-Si Schottky diodes (SDs) were determined by the measurement impedance technique. Dielectric properties and electrical conductivity of Au/(PVA/Ni,Zn acetates)/*n*-Si SDs in the frequency range of 0.5 kHz to 10 MHz and voltage range of −2 to 5 V were investigated in detail using experimental *C–V* and *G–V* measurements. Experimental results show that the values of the dielectric constant (ε′), dielectric loss (ε″), and tan δ obtained from the measured capacitance and conductance have been a strong function of frequency and applied voltage, and the values of ε′ have been unexpectedly found to be negative, especially at high voltages. Other parameters of Au/(PVA/Ni,Zn acetates)/*n*-Si SDs, such as ac electrical conductivity (σ_{ac}), the real part of electric modulus (M'), and the imaginary part of electric modulus (M'') varied with changing frequency for various voltages. The main propose of this study is to discuss the polymeric interfacial layer at metal and semiconductor affect and probe the dielectric properties of Au/(PVA/Ni,Zn acetates)/*n*-Si SDs regarding the negative capacitance as a function of frequency and voltage. © 2011 Wiley Periodicals, Inc. J Appl Polym Sci 122: 265–272, 2011

Key words: Au/(PVA/Ni,Zn acetates)/*n*-Si; polyvinyl alcohol; dielectric properties; electrospinning technique

INTRODUCTION

Schottky contacts are important in the performance of semiconductor devices for various electronic and optoelectronic applications. Many researchers have extensively investigated interfacial parameters, such as the interface states and interfacial layer, because these cause strong masking of the electrical characteristics of the Schottky barrier diodes (SBDs).[1–8] In recent years, considerable attention was given the fabrication and electrical characterization of organic semiconductor devices such as Schottky diodes (SDs), transistors, *p-n* junctions and solar cell.[9–22] There are many reports of conjugated conducting polymers in the field of electronics and optoelectronics. Among the various conducting polymers, poly(vinyl alcohol) (PVA), polyaniline, poly(alkylthiophene)polypyrrole, polyophene, and poly(3-hexylthiophene) became an attractive research topic among chemists, physicists, and electrical engineers alike, owing to their potential applications and interesting properties.[16,17,20,23–30] Investigating various SDs fabricated with different interfacial layer, especially a polymeric interfacial layer is important for understanding of the electrical and dielectrical properties of Schottky contacts. For this reason, PVA film was used in this study as an interfacial layer between metal and semiconductor.

PVA is an interesting synthetic polymer because it is water soluble and biocompatible, which are mainly due to hydrogen bonds between hydroxyl groups on the chain and water molecules or biomolecules.[31] The hydrogen bonding between hydroxyl groups plays an important role in the properties of PVA, such as its wide crystallinity range, and high crystal modulus.[32] The important features of semicrystalline PVA are the presence of crystalline and amorphous regions and its physical properties, which result from the crystal-amorphous interfacial effect.[33] Many physicists and chemists have devoted their efforts in studying and improving the electrical properties of polymers doped with metal ions.[30,34–47] When a polymer is doped, the dopant can induce modifications in the molecular structure and hence the microstructural property of the polymer. In particular, the transition metal salts and nanoparticle-doped polymers are considered to be a new class of organic materials due to their considerable modification on physical properties including microstructural, optical, electrical, and thermal properties. These changes in physical properties, depends on

Correspondence to: T. Tunç (tctunc@gmail.com).

the chemical nature of the dopant and the way in which they interact with the host polymer.[34]

The incorporation of metal chlorides ($CoCl_2$, $CuCl_2$, and $FeCl_3$) into poly(vinyl chloride) (PVC) and PVA produced intensity changes in infrared absorption bands of the polymers and resulted in a 10^6-fold increase in the electrical conductivity of the films.[40–42] These effects resulted in a new, specific metal–polymer interaction, for which a model based on strong electrical coupling between the metal atoms and polar C—Cl and C—OH bonds of PVC and PVA, respectively, was presented.[41,42]

The electrical characteristics of Shottky diodes are generally related by its interface quality. The existence of such an interfacial layer can have a strong influence on the diode characteristics. Investigating various SDs fabricated with different interfacial layer, especially a polymeric interfacial layer, is important for understanding of the electrical and dielectrical properties of Schottky contacts. For this reason, PVA film was used in this study as an interfacial layer between metal and semiconductor.

In this work, we prepared composites of PVA and inorganic salts as interfacial layer, nickel and zinc acetate, to investigate the effect of the inorganic salts concentration on the dielectric constant (ε') values and alternating-current (ac) conduction mechanisms of PVA to improve the properties of PVA to make it more applicable. Thus, PVA added with different ratios of nickel and zinc was produced and PVA/Ni,Zn acetates nanofiber film on silicon semiconductor was fabricated by the use of an electrospinning technique. Electrospinning utilizes electrical force to produce polymer fibers. This process consists of four major components: A high-voltage power supply, a spinneret, a syringe pump, and an electrically conductive collector. The syringe pump is an important component of the process, to achieve a constant and adjustable feed-rate of the polymeric solution.[43] A simple illustration of the electrospinning system is given in Figure 1. This polymer was used the fabrication of Au/(PVA/Ni,Zn acetates)/*n*-Si SDs as an interfacial layer in this study.

In our previous work, the electrical and dielectric properties of Au/(PVA/Ni,Zn acetates)/*n*-Si SDs were studied in the temperature range of 80–400 K.[44] The main aim of this study, however, is to probe the dielectric properties of Au/(PVA/Ni,Zn acetates)/*n*-Si SDs regarding the negative capacitance (NC) as a function of frequency and voltage.

EXPERIMENTAL

In this work, 350-μm thick *n*-type (phosphor doped) Si wafer with (111) orientation and 0.7 Ω-cm resistivity was used as substrate. Before producing contacts, the Si wafer was first cleaned in a mixture of a per-

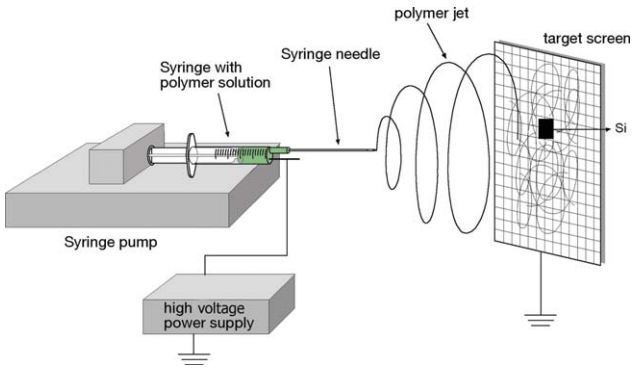

Figure 1 Schematic representation of the electrospinning process. [Color figure can be viewed in the online issue, which is available at wileyonlinelibrary.com.]

oxide-ammoniac solution for 10 min, then in H_2O + HCl solution and was then rinsed in deionized water for 15 min using an ultrasonic bath. After surface cleaning, high-purity Al with a thickness of $\sim$ 2000 Å was thermally evaporated onto whole back side of the Si wafer at a pressure $\sim 10^{-6}$ Torr in a high-vacuum system. The ohmic contacts were formed by annealing them for a few minutes at 450°C.

A total of 0.5 g of nickel acetate and 0.25 g of zinc acetate were mixed with 1 g of PVA (molecular weight = 72,000) and 9 mL of deionized water. After vigorous stirring for 2 h at 50°C, a viscous solution of PVA/Ni,Zn acetates was obtained. Using a peristaltic syringe pump, the precursor solution was delivered to a metal needle syringe (10 mL) with an inner diameter of 0.9 mm at a constant flow rate of 0.02 mL/h. The needle was connected to a high-voltage power supply and positioned vertically on a clamp. A piece of flat aluminum foil was placed 15 cm below the tip of the needle to collect the nanofibers. The Si wafer was placed on the aluminum foil. Upon applying a high voltage of 20 kV to the needle, a fluid jet was ejected from the tip. The solvent evaporated and a charged fiber was deposited onto the Si wafer as a nonwoven mat. After spinning, the Schottky/rectifier contacts were coated by evaporation with Au dots with a diameter of $\sim$ 1.0 mm (diode area = 7.85×10^{-3} cm^2).

Before fabricating the rectifying contact, the film of electrospun PVA composite fibers added with different ratios of nickel and zinc, which was deposited onto the Si wafer, was examined using a scanning electron microscope (SEM). The scanning electron microscopy measurements were recorded on a Quanto 400 FEI MK-2 microscope. The chemical compositions were recorded by energy dispersive spectroscopy (EDS). Figure 2 shows the peaks belonging to elements detected by EDS analysis. C, O, Ni, and Zi peaks arise from PVA and dopants. The thermal properties of the electrospun nanofibers

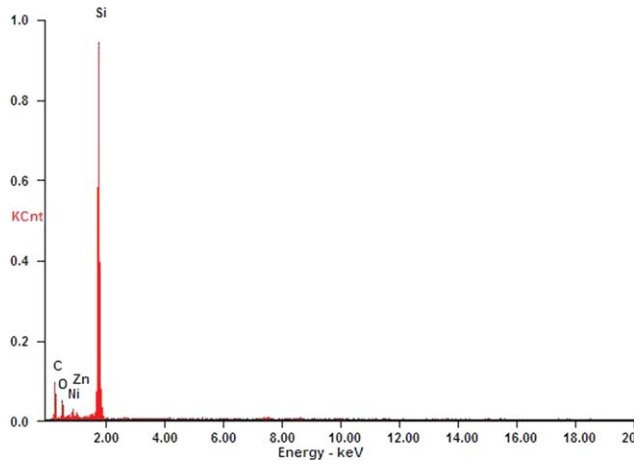

Figure 2 EDS spectrum of the (PVA/Ni,Zn) nanofibers. [Color figure can be viewed in the online issue, which is available at wileyonlinelibrary.com.]

were elucidated by the use of Schimadzu DSC-60 differential scanning calorimetry (DSC) instrument. The sample was first heated to 200°C under nitrogen atmosphere and cooled down to room temperature. The sample was then heated up to 500°C at a rate of 10°C/min. The results are given in Figure 3. As seen from Figure 3, the melting and glass transition temperatures of (PVA/Ni,Zn acetates) nanofibers are 197 and 240°C, respectively, and the thermal degradation starts at 422°C.

The capacitance–voltage–frequency (*C–V–f*) and conductance–voltage–frequency (*G/w–V–f*) characteristics of the diodes were measured in the frequency range of 5 kHz to 10 MHz by using HP 4192 A LF impedance analyzer (5 Hz to 13 MHz) and the test signal of 40 $mV_{rms.}$. All measurements were carried out at room temperature.

RESULTS AND DISCUSSION

The frequency dependence of dielectric constant (ε'), dielectric loss (ε''), loss tangent (tan δ), and ac electrical conductivity (σ_{ac}) were evaluated from the knowledge of capacitance (C) and conductance (G/w) for Au/(PVA/Ni,Zn acetates)/*n*-Si SDs in the frequency range of 0.5 kHz to 10 MHz. The values of ε', ε'', tan δ, and σ_{ac} of the samples were determined from following expressions, respectively.[48–51]

$$\varepsilon' = \frac{C}{C_o} = \frac{Cd_i}{\varepsilon_o A} \quad (1)$$

$$\varepsilon'' = \frac{G}{\omega C_o} = \frac{Gd_i}{\varepsilon_o \omega A} \quad (2)$$

$$\tan\delta = \frac{\varepsilon''}{\varepsilon'} \quad (3)$$

$$\sigma_{ac} = \varepsilon' \omega \varepsilon_o \tan\delta \quad (4)$$

where the quantities of d, ε_0, and ω ($= 2\pi f$) are the thickness of the polymer, permittivity of free space, and A the area of the upper electrode, respectively.

The terms complex electric modulus (M^*) formalisms with regard to the analysis of the dielectric or polymer materials have so far been discussed by several authors, most of whom have preferred electric modulus in defining the dielectric property and conduction mechanism of these materials.[52,53] The values of real (M') and imaginary parts (M'') of M^* of the samples were also determined from following expressions, respectively.[52,53]

$$M^* = \frac{1}{\varepsilon^*} = M' + jM'' = \frac{\varepsilon'}{\varepsilon'^2 + \varepsilon''^2} + j\frac{\varepsilon''}{\varepsilon'^2 + \varepsilon''^2} \quad (5)$$

The real component M' and the imaginary component M'' are calculated from ε' and ε''.

Figure 4 shows the voltage dependence of the real part of dielectric constant (ε') of the Au/(PVA/Ni,Zn acetates)/*n*-Si SD at various frequencies. It is noticed that the values of ε' decrease with increasing frequency and tend to become negative. The decrease in ε' with increasing frequency may be attributed to the polarization decreasing with increasing frequency. The negative value of dielectric constant was observed due to the NC in forward bias.

The NC phenomenon in various devices, such as inorganic SDs, inorganic homojunction photodetectors has been reported previously, while its origin is still under debate.[54–60] Several suggestions have been proposed for the exact reason of NC. For instance, Wu et al.[54] ascribed excess negative and positive capacitances at abrupt SDs to interface charges and a "waterfall" of electrons "falling off the Schottky barrier cliff". They pointed out that such strange admittances were not related to interface charge at the front Schottky contact but to defective

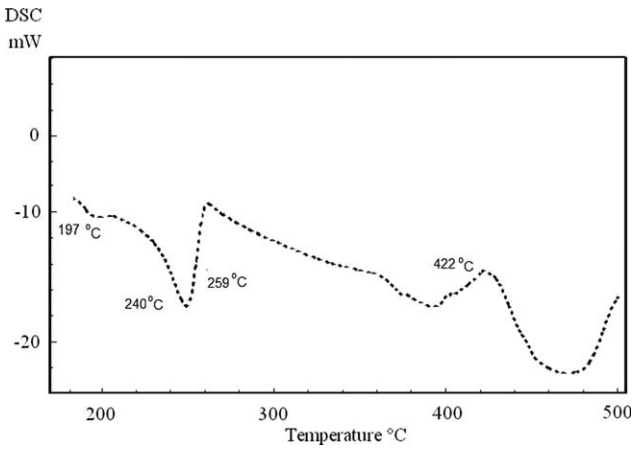

Figure 3 DSC curve of the (PVA/Ni,Zn) nanofibers.

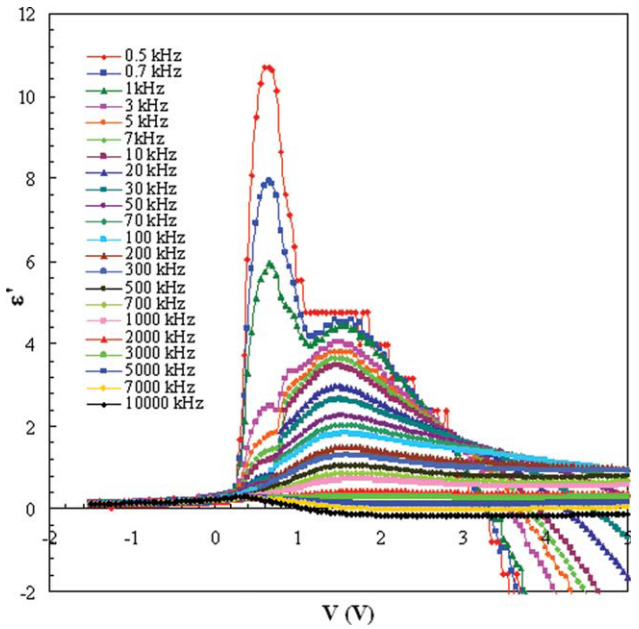

Figure 4 The variations of the dielectric constant versus applied voltage for various frequencies of Au/(PVA/Ni,Zn)/*n*-Si structure at room temperature. [Color figure can be viewed in the online issue, which is available at wileyonlinelibrary.com.]

back contacts. But, Werner et al.[55] had a strong disagreement with the interpretation of Wu et al. They attributed to the capacitance and inductance to excessive minority-carrier extraction at defective back contacts. Jones et al.[57] claim that the observed NC mechanism stems from the relaxation-like nature of the material. According to Jones et al.,[57] relaxation-like material is responsible from NC due to injection of holes which recombine easily with the electron free carriers of the dipole near the junction and hence decrease the charge dipole. This mentioned process produces a large NC effect because the recombination process is strong and the charges involved are so close to the contact charges. Champness and Clark[61] claim that the NC arise from the inductive behavior of materials. According to them, the NC caused by the injection of minority carriers can be observed only at forward applied bias voltage.

Also, NC has been previously observed and modeled the existence of NC in organic polymers, organic light emitting devices, and more.[62–70] Martens et al.[62] were able to explain satisfactorily the observed NC effect as caused by a distribution of relaxation times under different bias conditions. Their model was based on space charge transport and Poisson equation using frequency dependent carrier mobility. In another work,[63] the authors reported NC effect in OC_1C_{10}-PPV polymers where both electrons and holes were assumed to be present. Equivalent circuit models were used to explain the results in different bias regimes. Kwok[66] has examined the capacitance effect in organic polymers using the Drude model. His results suggested that it was possible to account for the capacitance effect in organic polymers using the Drude model provided he makes adjustment for dispersion of the carriers. This was modeled using a complex mobility parameter. He compared the simulation results of his model with data reported in the literature.[63] He was able to extract values of the carrier densities and the carrier mobilities and these values are in general agreement with those reported in the open literature. On the other hand, the detail of the NC and dielectric constant at the reverse bias requires further research.

The dispersion in ε' with frequency can be explained by Maxwell–Wagner type interfacial polarization, i.e., the fact that inhomogeneities give rise to a frequency dependence of the conductivity because charge carriers accumulate at the boundaries of less conductive regions, thereby creating interfacial polarization.[50] Figures 5 and 6 show the voltage dependence of dielectric loss (ε'') and the loss tangent (tan δ) of the Au/(PVA/Ni,Zn acetates)/*n*-Si SD at various frequencies. As can be seen in these figures, the values of ε'' and tan δ are strongly dependent on both frequency and applied

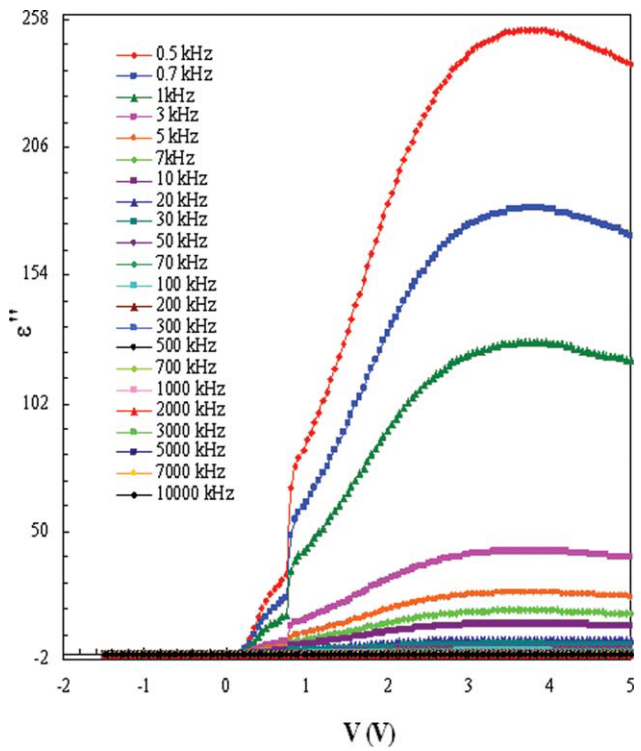

Figure 5 The variations of dielectric loss versus applied voltage for various frequencies of Au/(PVA/Ni,Zn)/*n*-Si structure at room temperature. [Color figure can be viewed in the online issue, which is available at wileyonlinelibrary.com.]

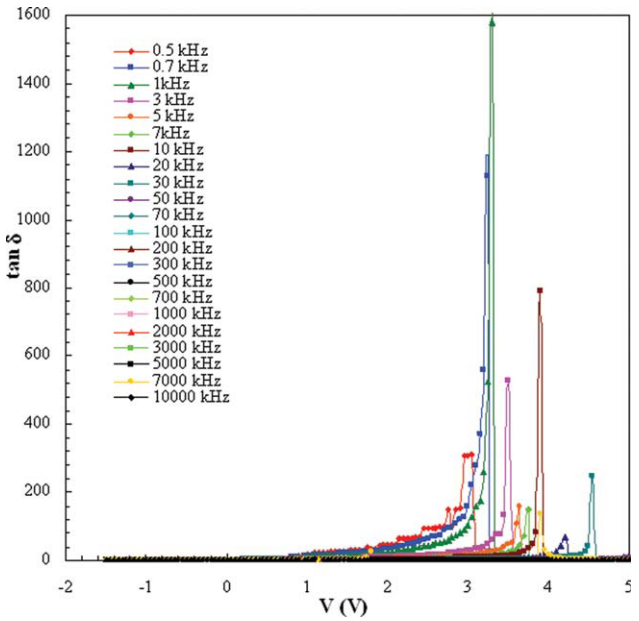

Figure 6 The variations of tangent loss versus applied voltage for various frequencies of Au/(PVA/Ni,Zn)/*n*-Si structure at room temperature. [Color figure can be viewed in the online issue, which is available at wileyonlinelibrary.com.]

bias voltage. The ε′–*V*, ε″–*V*, and tan δ–*V* characteristics have a peak, especially at low frequency. The peak value of the ε′ and ε″ stem from measurements of capacitance and conductance values, respectively. Therefore, the peak behavior of the ε′, ε″, and tan δ can depend on a number of parameters, such as doping concentration, interface state of diode, and the thickness of the interfacial insulator layer.[3] It is well known that capacitance and conductance are extremely sensitive to the interface properties, due to the fact that the interface states respond differently to low and high frequencies.[3–8] Similar results have been reported in the literature[3,8,47–50] and ascribed such a peak only to interface states.

The frequency dependence of ε′, ε″, and tan δ of Au/(PVA/Ni,Zn acetates)/*n*-Si SD at different voltage are presented in Figure 7(a–c), respectively. The values of ε′, ε″ and tan δ obtained from the measured capacitance and conductance were a strong function of applied voltage, especially at low frequencies. As shown in Figure 7(a), the values of ε′ show a steep decrease with increasing frequency at low voltages. However, the ε′–*V* characteristics show a peak at high voltages. The values of ε″ decrease with increasing frequency at low frequencies. Also, it is clearly seen in Figure 7 that the values of ε′, ε″, and tan δ of Au/(PVA/Ni,Zn acetates)/*n*-Si SD are almost independent of voltage at high frequencies. In principle, at low frequencies, dipolar and interfacial or surface polarization contribute to the values of ε′ and ε″.[61,71]

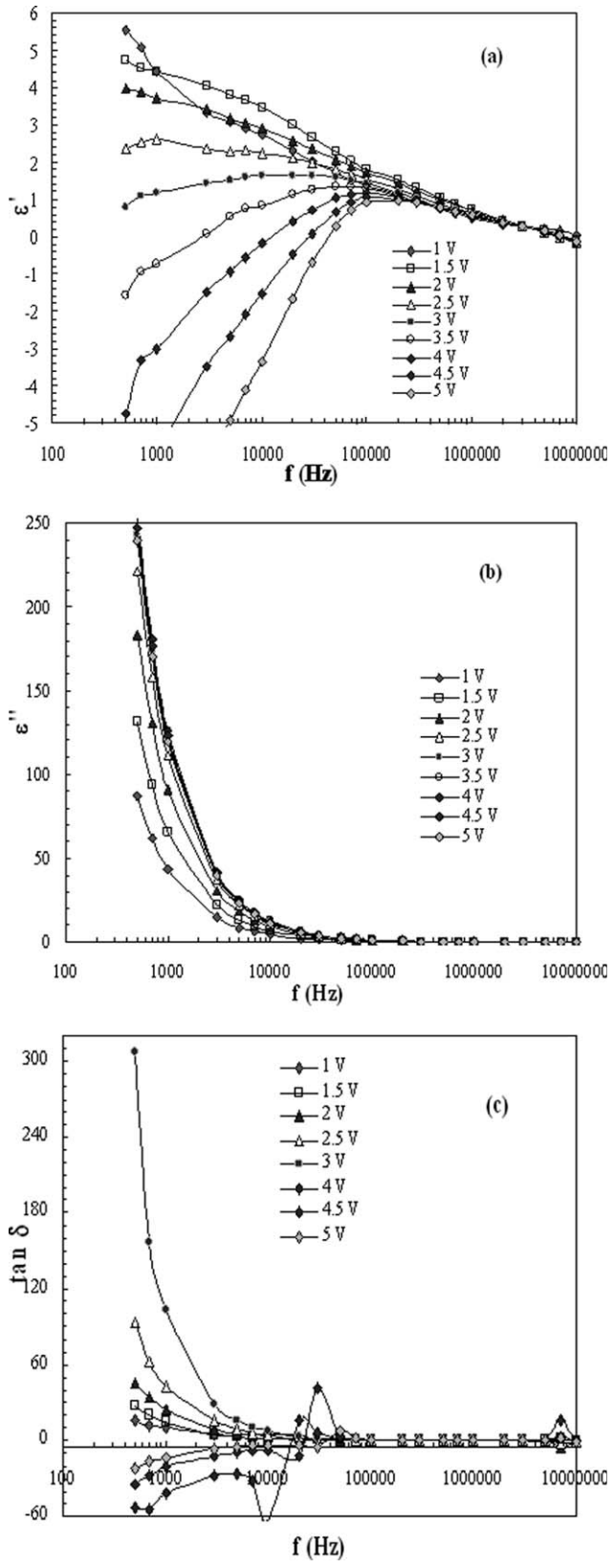

Figure 7 Frequency dependence of the (a) ε′, (b) ε″, and (c) tan δ for various applied voltage of Au/(PVA/Ni,Zn)/*n*-Si structure at room temperature.

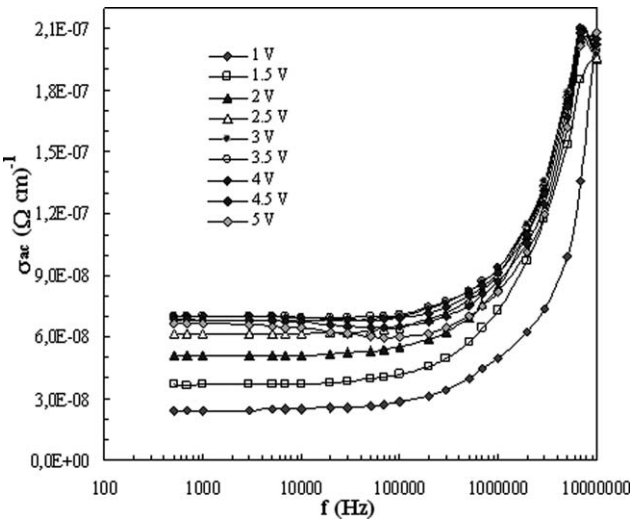

Figure 8 Frequency dependence of ac electrical conductivity (σ_{ac}) for various applied voltage of Au/(PVA/Ni,Zn)/*n*-Si structure at room temperature.

The behavior of σ_{ac} of the Au/(PVA/Ni,Zn acetates)/*n*-Si SD at various voltages is presented in Figure 8. It was noted that the electrical conductivity generally increases with increasing frequency, especially at high frequencies up to $\sim$ 100 kHz. This electrical conductivity contributes only to the dielectric loss, which becomes infinite at zero frequency, and is not important at high frequencies. As the frequency increases, electrical conductivity increases because the polarization decreases with increasing frequency. The increase of electrical conductivity leads to an increase in the eddy current which, in turn, increases the energy loss tan δ. This result corresponds with the decreasing value of ε'' with increasing frequency.

Moreover, the negative value of the dielectric constant may be caused by the injection of charge carriers due to the structure of PVA added Ni, Zn nanofiber film at the interface, but the detailed physical mechanisms of injection are not well understood at present. To further investigate this polymeric interface film, the morphology of the PVA composite electrospun fibers added with Ni and Zn were determined by using SEM.

Figure 9(a,b) shows the SEM images of PVA/Ni,Zn acetates nanofibers. It can be seen that nanofibers are different diameters. The fibers can be seen to be elongated and straight, with relatively homogeneous diameters, ranging from 150 to 900 nm. When the amount of Zn acetate in PVA solutions was increased, the conductivity of the polymer was observed to decrease, as given in Table 1 of Ref. 43.

Figure 10(a,b) shows the variation of the real part of electric modulus, M', and the imaginary part, M'', of Au/(PVA/Ni,Zn acetates)/*n*-Si SD as a function of frequency at various bias voltages at room temperature. It is evident from Figure 10 that M' reaches a maximum value at higher frequency, corresponding to $M_\infty = 1/\varepsilon_\infty$ due to the relaxation process. At low frequencies, the values of M' tend to approach zero, confirming the removal of electrode polarization. The M'' of electric modulus M^* versus f have a peak for each voltage [Fig. 10(b)] at certain frequency regions. Generally, M'' increases with increasing frequencies. Similar results have been reported in the literature.[46,48]

Figure 11 shows the M'' versus M' plots for various applied bias voltages. As can be seen in this figure, each M'' versus M' plot gives a peak at low frequency (about $\sim$ 3 kHz). The peak value increases with increasing bias voltage. The semicircles in the

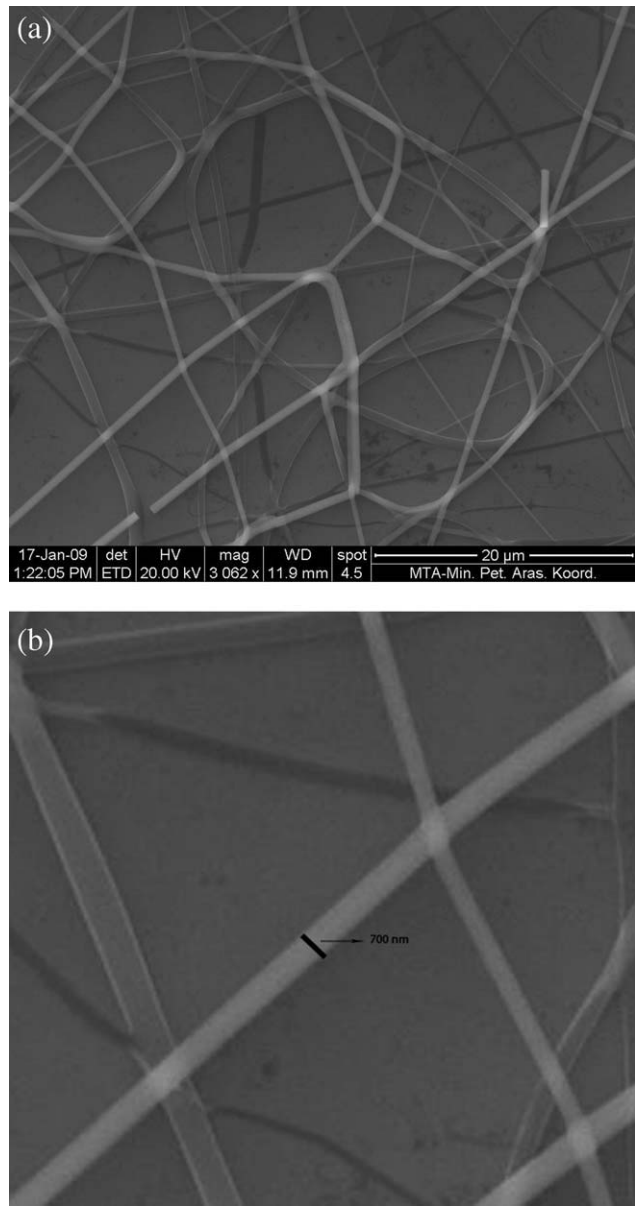

Figure 9 (a) SEM picture of PVA/Ni,Zn nanofibers and (b) magnification of the SEM of PVA/Ni,Zn nanofibers.

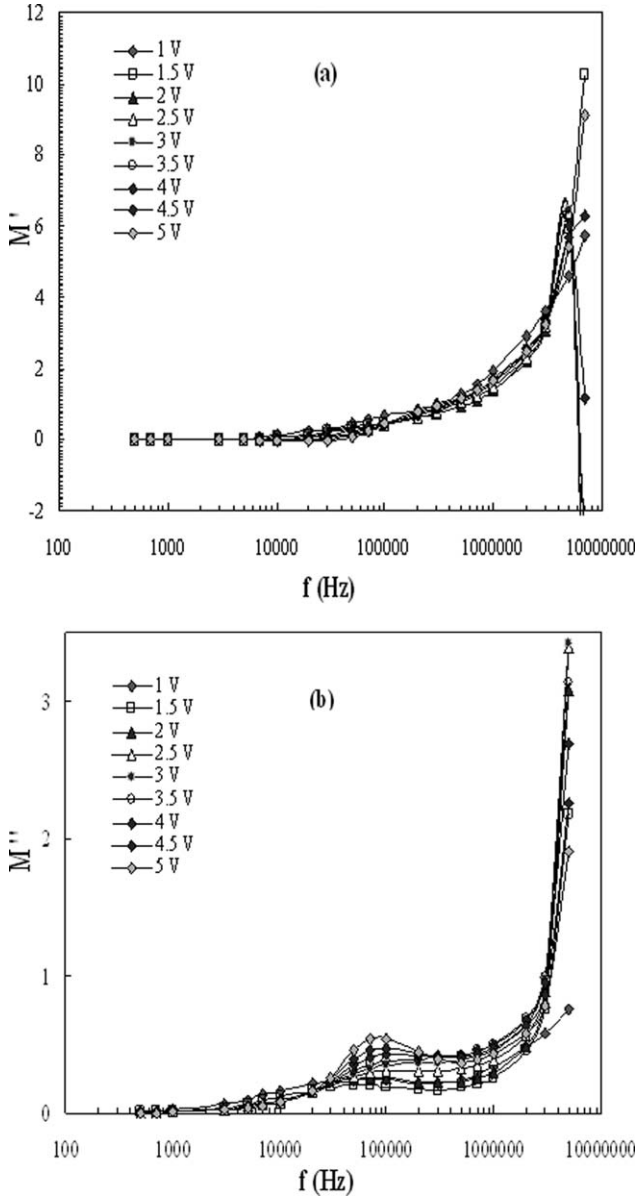

Figure 10 (a) The real part M' and (b) the imaginary part M'' of electric modulus M^* versus frequency for Au/(PVA/Ni,Zn)/*n*-Si structure at room temperature.

Cole–Cole diagram of electric modulus arise from the relaxation processes especially at low frequencies. The interfacial polarization is more sensitive in the low frequency and may even extend to few kilohertz ranges and it occurs when mobile charge carriers are impeded by a physical barrier that inhibits charge migration.

CONCLUSIONS

This study analyzed the dielectric characteristics of Au/(PVA/Ni,Zn acetates)/*n*-Si SDs. The experimental results show that, while the values of dielectric constant (ε') decrease with increasing frequency, especially at low voltage, the ac electrical conductivity increases with increasing frequency due to the fact that the polarization is decreasing with increasing frequency. It is conceivable that the ε' value decreases with decreasing polarization and more carriers are introduced in the structure. These results can be attributed to an increase in the eddy current caused by additional charge carriers, due to the origin of the structure of PVA added Ni, Zn nanofiber film at interface. The real part of electric modulus (M') and the imaginary part of electric modulus (M'') increase with increasing frequency. These behaviors are related to the polarization decreasing with increasing frequency in the PVA/Ni,Zn interface. It is concluded that the dielectric properties of PVA/Ni,Zn acetates polymeric layer in Au/(PVA/Ni,Zn acetates)/*n*-Si SD are strongly dependent on both the frequency and applied bias voltage. The attractive side of our experimental results is that the observed negative values of ε' correspond to the maximum of the device conductance. The capacitance should always be positive in the frequency domain. On the contrary, if at some time the current increases, then the capacitance could be negative in a certain range of frequencies. A current that increases in time after application of a voltage step has been ascribed to several phenomena, including two carrier space charge limited currents, modification of traps population, injection through intermediate surface states, and modification of electronic barrier heights at grain boundaries (polycrystalline materials) or at the junction of diode. Therefore, it is proposed that NC is due to a decrease in the

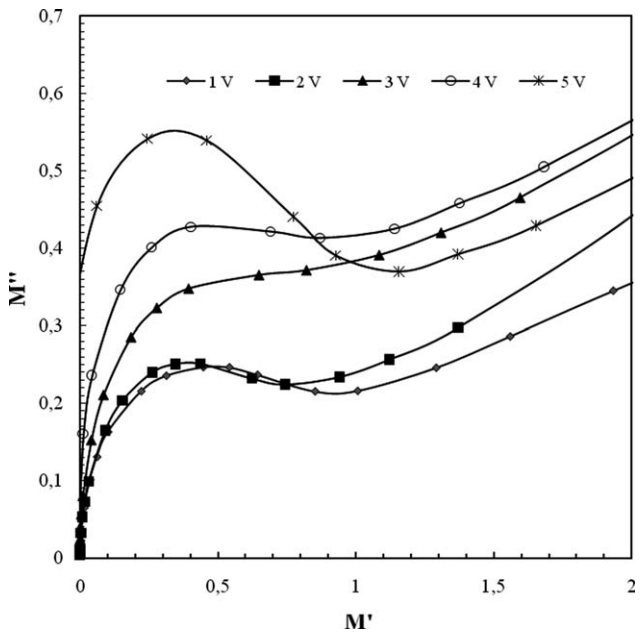

Figure 11 Cole–Cole plots Au/(PVA/Ni,Zn)/*n*-Si structure at room temperature.

Schottky barrier width at the metal–dielectric interface.[71]

This work is supported by Gazi University Scientific Research Project numbered 04/2010-27.

References

1. Rhoderick, E. H.; Williams, R. H. Metal-Semiconductor Contacts; Oxford: Cleredon, 1988.
2. Werner, J. H. Appl Phys 1988, A47, 291.
3. Afandiyeva, İ. M.; Dökme, İ.; Altındal, Ş. Microelectron Eng 2008, 85, 365.
4. Passlack, M.; Hong, M.; Mannaerts, J. P. Solid-State Electron 1996, 39, 1133.
5. Dökme, İ.; Altındal, S.; Afandiyeva, İ. M. Semicond Sci Technol 2008, 23, 035003.
6. Dökme, İ. Physica B 2007, 388, 10.
7. Sahin, M.; Durmus, H.; Kaplan, R. Appl Surf Sci 2006, 252, 6269.
8. Dökme, İ.; Altındal, Ş. Physica B 2007, 393, 328.
9. Ebeoğlu, M. A.; Kılıçoğlu, T.; Aydın, M. E. Physica B 2007, 395, 93.
10. Vural, Ö.; Yıldırım, N.; Altındal, S.; Türüt, A. Synth Met 2007, 157, 679.
11. Lungenschmied, C.; Ehrenfreund, E.; Sariciftci, N. S. Org Electron 2009, 10, 115.
12. Reddy, V. S.; Karak, S.; Ray, S. K.; Dhar, A. Org Electron 2009, 10, 138.
13. Katsia, E.; Tallarida, G.; Kutrzeba-Kotowska, B.; Ferrari, S.; Bundgaard, E.; Søndergaard, R.; Krebs, F. C. Org Electron 2008, 9, 1044.
14. Kawabe, E.; Yamane, H.; Sumii, R.; Koizumi, K.; Ouchi, Y.; Seki, K.; Kanai, K. Org Electron 2008, 9, 780.
15. Sharma, G. D.; Sharma, S.; Roy, M. S. Solar Energy Mat Solar Cell 2003, 80, 131.
16. Benor, A.; Knipp, D. Org Electron 2008, 9, 209.
17. Girotto, C.; Cheyns, D.; Aernouts, T.; Banishoeib, F.; Lutsen, L.; Cleij, T. J.; Vanderzande, D.; Genoe, J.; Poortmans, J.; Heremans, P. Org Electron 2008, 9, 740.
18. Yakuphanoğlu, F. Synth Met 2008, 158, 108.
19. Temirci, C.; Çakar, M.; Türüt, A.; Onganer, Y. Phys Stat Sol (a) 2004, 201, 3077.
20. Aydoğan, Ş.; Sağlam, M.; Türüt, A. Polymer 2005, 46, 563.
21. Güllü, Ö.; Aydoğan, S.; Türüt, A. Microelectron Eng 2008, 85, 1647.
22. Güllü, Ö.; Barıs, Ö.; Biber, M.; Türüt, A. Appl Surf Sci 2008, 254, 3039.
23. Gupta, R. K.; Singh, R. A. Mater Chem Phys 2004, 86, 279.
24. Gupta, R. K.; Singh, R. A. Mat Sci Semicon Proc 2004, 7, 83.
25. Abdalla, T. A.; Mammo, W.; Workalemahu, B. Synth Met 2004, 144, 213.
26. Campbell, A.; Bradley, J. D. C.; Werner, E.; Brütting, W. Synth Met 2000, 111, 273.
27. Ahmed, F. E.; Yassin, O. A. Microelectron J 2007, 38, 834.
28. Kaneto, K.; Nakagawa, M.; Takashima, W. Curr Appl Phys 2004, 4, 206.
29. Huang, L. M.; Wen, T. C.; Gopalan, A. Thin Solid Film 2005, 473, 300.
30. Nguyen, N. C.; Potje-Kamloth, K. Thin Solid Film 1999, 338, 142.
31. Hoffman, A.; Ann, N. Y. Acad Sci 2001, 62, 944.
32. Shibayama, M.; Sato, M.; Kimura, Y.; Fujiwara, H.; Nomura, S. Polymer 1988, 29, 336.
33. Pawde, S. M.; Deshmukh, K.; Parab, S. J Appl Polym Sci 2008, 109, 1328.
34. Bhajantri, R. F.; Ravindrachary, V.; Harisha, A.; Ranganathaiah, C.; Kumaraswamy, G. N. Appl Phys A 2007, 87, 797.
35. Kubo, J.; Rahman, N.; Takahashi, N.; Kawai, T.; Matsuba, G.; Nishida, K.; Kanaya, T.; Yamamoto, M. J Appl Polym Sci 2009, 112, 1647.
36. Bouropoulos, N.; Psarras, G. C.; Moustakas, N.; Chrissanthopoulos, A.; Baskoutas, S. Phys Stat Sol (a) 2008, 205, 2033.
37. Ahmed, M. A.; Abo-Ellıl, M. S. J Mater Sci-Meter El 1998, 9, 391.
38. Hanafy, T. A. J Appl Polym Sci 2008, 108, 2540.
39. Shehap, A.; Abd Allah, R. A.; Basha, A. F.; Abd El-Kader, F. H. J Appl Polym Sci 1998, 68, 687.
40. Rao, T. V.; Chopra, K. L. Thin Solid Films 1979, 60, 387.
41. El Kader, F. H.; Attia, G.; Ibrahim, S. S. Polym Degrad Stab 1994, 43, 253.
42. Tawansi, A.; El Kodary, A.; Abdelnaby, M. M. Curr Appl Phys 2005, 5, 572.
43. Uslu, I.; Baser, B.; Yaylı, A.; Aksu, M. L. e-Polymers 2007, 145.
44. Dökme, İ.; Altındal, S.; Tunç, T.; Uslu, İ. Microelectron Reliab 2010, 50, 39.
45. Saito, H.; Stuhn, B. Polymer 1994, 35, 475.
46. Mossad, M. M. J Mater Sci (a) 1990, 121, 119.
47. Salama, A. H.; Dawys, M.; Nada, A. M. A. Polym-Plast Technol 2004, 43, 1067.
48. Symth, C. P. Dielectric Behaviour and Structure; McGraw-Hill: New York, 1955.
49. Mattsson, M. S.; Niklasson, G. A.; Forsgren, K.; Harsta, A. J. Appl Phys 1999, 85, 2185.
50. Chelkowski, A. Dielectric Physics; Elsevier: Amsterdam, 1980.
51. Nicollian, E. H.; Brews, J. R. MOS Physics and Technology; Wiley: New York, 1982.
52. Prabakar, K.; Narayandass, S. K.; Mangalaraj, D. Phys Stat Sol (a) 2003, 199(3),507.
53. Migahed, M. D.; Ishra, M.; Fahmy, T.; Barakat, A. J. Phys Chem Solids 2004, 65, 1121.
54. Wu, X.; Yang, E. S.; Evans, H. L. J Appl Phys 1990, 68, 2845.
55. Werner, J. H. J Appl Phys 1991, 70, 1087.
56. Ershov, M.; Liu, H. C.; Li, L.; Buchanan, M.; Wasilewski, Z. R.; Ryzhii, V. Appl Phys Lett 1997, 70, 1828.
57. Jones, B. K.; Santana, J.; McPherson, M. Solid State Commun 1998, 107, 47.
58. Lemmi, F.; Johnson, N. M. Appl Phys Lett 1999, 74, 250.
59. Kavasoglu, A. S.; Kavasoglu, N.; Kodolbas, A. O.; Birgi, O.; Oktu, O.; Oktik, S. Microelectron Eng 2010, 87, 108.
60. Zhu, C. Y.; Feng, L. F.; Wang, C. D.; Cong, H. X.; Zhang, G. Y.; Yang, Z. J.; Chen, Z. Z. Solid State Electron 2009, 53, 324.
61. Champness, C. H.; Clark, W. R. Appl Phys Rev Lett 1990, 56, 1104.
62. Martens, H. C. F.; Huiberts, J. N.; Blom, P. W. M. Appl Phys Lett 2000, 77, 1852.
63. Martens, H. C. F.; Pasveer, W. F.; Blom, H. B.; Huiberts, J. N.; Blom, P. W. M. Phys Rev B 2001, 63, 125328.
64. Castro, F. A.; Bueno, P. R.; Graeff, C. F. O.; Nüesch, F.; Zuppiroli, L.; Santos, L. F.; Faria, R. M. Appl Phys Lett 2005, 013505, 87.
65. Ehrenfreund, E.; Lungenschmied, C.; Dennler, G.; Neugebauer, H.; Sariciftci, N. S. Appl Phys Lett 2007, 012112, 91.
66. Kwok, H. L. Solid State Electron 2003, 47, 1089.
67. Pingree, L. S. C.; Scott, B. J.; Russell, M. T.; Marks, T. J.; Hersam, M. C. Appl Phys Lett 2005, 073509, 86.
68. Lai, P. Y.; Chen, J. S. J Appl Phys 2008, 033916, 104.
69. Bisquert, J.; Garcia-Belmonte, G.; Pitarch, A.; Bolink, H. J Chem Phys Lett 2006, 422, 184.
70. Bakueva, L.; Konstantatos, G.; Musikhin, S.; Ruda, H. E.; Shik, A. Appl Phys Lett 2004, 85, 3567.
71. El Kamel, F.; Gonon, P.; Jomni F.; Yangui, B. Appl Phys Lett 2008, 93, 042904-1.